

Electronic transport in thin films of BaPbO₃: Unraveling two-dimensional quantum effects

P. Seiler, R. Bartel, T. Kopp, and G. Hammerl*

*Center for Electronic Correlations and Magnetism, Experimental Physics VI,
Institute of Physics, University of Augsburg, 86135 Augsburg, Germany*

(Dated: September 26, 2019)

Recently, perovskite related BaPbO₃ has attracted attention due to its hidden topological properties and, moreover, has been used as a thin layer in heterostructures to induce two-dimensional superconductivity. Here we investigate the normal state electronic transport properties of thin films of BaPbO₃. Temperature and magnetic field dependent sheet resistances are strongly affected by two-dimensional quantum effects. Our analysis decodes the interplay of spin-orbit coupling, disorder, and electron-electron interaction in this compound. Similar to recently discussed topological materials, we find that weak antilocalization is the dominant protagonist in magnetotransport, whereas electron-electron interactions play a pronounced role in the temperature dependence. A systematic understanding of these quantum effects is essential to allow for an accurate control of properties not only of thin films of BaPbO₃, but also of topological heterostructures.

I. INTRODUCTION

Oxide heterostructures serve as a new source of functionality by combining intrinsic physical properties of different compounds in epitaxially grown artificial materials^{1,2}. Novel intriguing qualities emerge from the tunability of coupled degrees of freedom like charge, spin and orbital degrees, or by reduced dimensionality³. Oxide heterostructures with their interfaces can do even more to realize multi-functional devices: as compared to, e.g., semiconductor heterostructures, they allow for emergent electronic phases that are not stable in the bulk. Such electronic phases can be well constrained on the nanoscale, often being correlated electronic systems driven by electronic reconstruction⁴⁻⁶. Moreover, the inversion symmetry is generically broken at these interfaces, leading to a strong Rashba-type spin-orbit coupling^{7,8} and inducing exotic spin textures or even superconducting states that are characterized by non-trivial values of topological invariants^{9,10}. Therefore, transport in these two-dimensional systems is intrinsically intriguing and quantum corrections have an immense impact on transport properties at low temperatures. Self-interference of extended electron waves or electron-electron interaction effects decide on metallic or insulating ground states. Specifically, disorder in two-dimensional systems causes weak localization^{8,11,12} and an insulating ground state^{13,14}, whereas its antagonist, weak antilocalization^{8,15,16}, originating from a combination of disorder and spin-orbit coupling, results in a metallic ground state. In this context of quantum transport, the two perovskite-related compounds BaBiO₃ and BaPbO₃ are promising candidates to be studied: both are expected to preserve a “hidden” topological insulator phase when electron or hole doped^{17,18}. In BaPbO₃-BaBiO₃ bilayers grown on SrTiO₃ substrates we recently observed two-dimensional superconductivity with maximum T_c of 3.5 K, presumably induced by interfacial strain where BaPbO₃ is acting as a dopant layer¹⁹. This is astounding as BaBiO₃ is a charge-density wave ordered

insulator²⁰⁻²², whereas BaPbO₃ a metal which becomes superconducting only at temperatures below 0.5 K²³.

To gain a better control and understanding of heterostructures involving BaPbO₃, we study the transport properties of a thin layer of BaPbO₃ on top of a SrTiO₃ substrate. Due to the strong spin-orbit coupling in BaPbO₃ layers, we expect a sizable weak antilocalization contribution in our samples at low temperatures. In this article, we show experimental data retrieved from magnetotransport measurements alongside the temperature dependence of the sheet resistance. Whereas metallic features of weak antilocalization dominate the magnetic field dependence, insulating features of electron-electron interaction predominate in controlling the temperature dependence of the resistance. It turns out that a thoughtful data analysis is necessary to explain the—at first sight contradicting—experimental results.

II. METHODS

A. Sample Growth

All thin films of BaPbO₃ were grown by pulsed laser deposition (PLD) using commercially available stoichiometric targets with purities of at least 99.95% at maximum achievable density. The surface of the targets were cleaned for each sample growth to maintain the quality of the samples. We used single crystalline 5 mm × 5 mm × 1 mm sized (001) oriented one-side polished SrTiO₃ crystals as substrates the surface of which were HF treated^{24,25} and annealed in oxygen in order to guarantee extensive TiO₂ termination. The substrates were fixed by silver paste on heating platforms before being transferred to the vacuum chamber. The substrates were heated to ≈ 552 °C either by resistive or laser heating controlled by pyrometers in about 45 min at an oxygen background pressure of at least 0.25 mbar. Our PLD system is equipped with a KrF excimer laser having a nominal fluency of 2 J cm⁻². During thin film growth of

BaPbO₃ the oxygen background pressure was leveled to ≈ 1 mbar. The laser pulse energy was set to 550 mJ for all samples and the laser shot frequency was limited to 3 Hz. After thin film deposition the samples were cooled to 400 °C within 3 min and annealed at an oxygen background pressure of ≈ 400 mbar for at least 20 min before they freely cooled to room temperature.

B. Sample Preparation

The topography of the samples was routinely checked by atomic force microscopy (AFM). The grown BaPbO₃ thin films only display (00*l*) oriented peaks in X-ray diffraction (XRD) experiments. We used X-ray reflectometry (XRR) to check the film thicknesses of the samples, where we found the expected linear dependence of the film thickness in respect to the number of laser pulses used during film synthesis. The samples were patterned using standard photolithography and argon ion-etching resulting in measurement bars of about 200 μm in length and 50 μm in width. Transport properties were measured in a commercial 14 T PPMS in common four-point geometry.

III. IMPACT OF QUANTUM CORRECTIONS

A. Quantum Interference

Due to the strong atomic spin-orbit coupling of lead, as well as the broken inversion symmetry of the interface, D'yakonov-Perel spin relaxation²⁶ is expected to affect transport in BaPbO₃ thin films. In combination with disorder, the spin relaxation results in a signature of weak antilocalization (WAL)²⁷⁻³¹, predicting a logarithmic decrease of the resistance upon cooling. In the presence of time-reversal symmetry breaking magnetic fields, the same correction causes a positive magnetoresistance that allows to extract the strengths of inelastic scattering as well as spin relaxation. An adequate description of the first order quantum correction to the conductivity of a two-dimensional system is given by the Iordanskii-Lyanda-Geller-Pikus theory^{16,32,33}. The specific magnetic field dependence is sensitive to the winding number of the spin expectation value traced along the Fermi surface. In the case of a triple spin winding, which has been identified in several SrTiO₃ based two-dimensional systems^{28,30,31} and is also in good agreement with our data, the Iordanskii-Lyanda-Geller-Pikus theory reproduces the analytical result of the Hikami-Nagaoka-Larkin theory⁸. The first order quantum correction to the conductivity in magnetic field B due to

quantum interference (QI) is given by

$$\delta\sigma^{\text{QI}}(B) = \frac{e^2}{\pi h} \left[\psi \left(\frac{1}{2} + \frac{B_{\text{so}} + B_i}{B} \right) - \frac{1}{2} \psi \left(\frac{1}{2} + \frac{B_i}{B} \right) + \frac{1}{2} \psi \left(\frac{1}{2} + \frac{2B_{\text{so}} + B_i}{B} \right) - \psi \left(\frac{1}{2} + \frac{B_o}{B} \right) \right], \quad (1)$$

with ψ being the digamma function. The effective magnetic fields are defined by

$$B_{\text{so}/i/o} = \frac{\hbar}{4eD\tau_{\text{so}/i/o}}, \quad (2)$$

with D being the diffusion constant, τ_o and τ_i the elastic and inelastic scattering times and τ_{so} the time scale associated with the D'yakonov-Perel spin relaxation³⁴.

For vanishing magnetic field, there are two relevant limits of Eq. (1): $B_{\text{so}} \gg B_i$, which relates to a metallic regime, and $B_{\text{so}} \ll B_i$, which corresponds to an insulating regime^{8,15}. The correction describing the metallic regime is given by

$$\delta\sigma^{\text{WAL}}(B \rightarrow 0) = -\frac{e^2}{2\pi h} \ln \left(\frac{B_o^2 B_i}{2B_{\text{so}}^3} \right). \quad (3)$$

By assuming an algebraic temperature dependence,

$$B_i = \gamma + \beta T^\alpha, \quad (4)$$

with temperature exponent α , the WAL quantum correction takes the form

$$\delta\sigma^{\text{WAL}}(T) = -\frac{e^2}{2\pi h} \ln \left(\frac{\gamma + \beta T^\alpha}{C^{\text{WAL}}} \right), \quad (5)$$

where C^{WAL} is a temperature independent constant. Equation (5) describes an increasing conductivity for decreasing temperature, indicating a metallic ground state. Note that the inelastic field does not necessarily vanish for zero temperature, due to a finite constant γ in Eq. (5). This has been observed in several magnetotransport measurements³⁵⁻³⁷. Also mind that the effect of spin-orbit coupling enters the conductivity correction in Eq. (5) only via the constant C^{WAL} , whereas the inelastic scattering processes are essentially responsible for the temperature dependence.

For the insulating case of weak localization (WL; $B_{\text{so}} \ll B_i$), Eq. (1) reduces to

$$\delta\sigma^{\text{WL}}(B \rightarrow 0) = \frac{e^2}{\pi h} \ln \left(\frac{B_i}{B_o} \right), \quad (6)$$

and in terms of a temperature dependent correction to the conductivity,

$$\delta\sigma^{\text{WL}}(T) = \frac{e^2}{\pi h} \ln \left(\frac{\gamma + \beta T^\alpha}{C^{\text{WL}}} \right). \quad (7)$$

Equation (7) describes a decrease of conductivity when the temperature is lowered and is the well-known logarithmic correction of WL.

We refer to the magnetoconductivity in magnetic fields $B \ll B_o$ as

$$\begin{aligned} \Delta\sigma^{\text{QI}}(B) &= \delta\sigma^{\text{QI}}(B) - \delta\sigma^{\text{QI}}(0) \\ &= \frac{e^2}{\pi h} \left[\Psi\left(\frac{B}{B_{\text{so}} + B_i}\right) - \frac{1}{2}\Psi\left(\frac{B}{B_i}\right) + \frac{1}{2}\Psi\left(\frac{B}{2B_{\text{so}} + B_i}\right) \right], \end{aligned} \quad (8)$$

where $\Psi(x) = \ln(x) + \psi\left(\frac{1}{2} + \frac{1}{x}\right)$. Note that in the metallic case ($B_{\text{so}} \gg B_i$), the conductivity up to quadratic order in the magnetic field is again driven by the inelastic scattering field, whereas the spin-orbit coupling fixes the prefactor,

$$\Delta\sigma^{\text{WAL}}(B) \approx -\frac{e^2}{\pi h} \frac{1}{48} \left(\frac{B}{B_i}\right)^2. \quad (9)$$

As the magnetic field and temperature dependence of the conductivity originates from the same analytic expression of the quantum correction, we emphasize that the appearance of WAL in terms of a positive magnetoresistance (following Eq. (9)) is intrinsically connected to a logarithmic decrease of the sheet resistance for lower temperature (following Eq. (5)).

B. Electron–Electron Interaction

A logarithmic increase in the sheet resistance for lower temperatures, however, cannot only be caused by WL, but also by electron–electron interaction (EEI) in the particle–hole channel. The corresponding correction to the conductivity in two dimensions is given by^{11,12,38}

$$\delta\sigma^{\text{EEI}}(T) = \zeta \frac{e^2}{\pi h} \ln\left(\frac{T}{C^{\text{EEI}}}\right), \quad (10)$$

where ζ is in the range between $\zeta = 1$ without screening and $\zeta \sim 0.35$ for perfect screening, and C^{EEI} is a temperature independent constant. Although the particle–hole channel is not sensitive to the magnetic field directly, a finite Zeeman splitting produces a magnetoconductivity following

$$\Delta\sigma^{\text{EEI}}(\tilde{B}) \approx -\frac{e^2}{\pi h} \frac{2(1-\zeta)}{3} \begin{cases} \ln\left(\frac{\tilde{B}}{1.3}\right) & \tilde{B} \gg 1 \\ 0.084\tilde{B}^2 & \tilde{B} \ll 1 \end{cases} \quad (11)$$

for $\tilde{B} = g\mu_B B/k_B T$. Therefore, magnetoresistance due to EEI is expected to grow monotonously with larger fields. This is in contrast with the decreasing magnetoresistance for higher magnetic fields in the case of WAL and, even more, with the negative progression of magnetoresistance for all magnetic fields in case of WL.

IV. EXPERIMENTAL RESULTS AND DISCUSSION

Magnetotransport data taken on various BaPbO₃ thin film samples show no indication of multi-band behavior (see Appendix A). This is an advantage over the more complicated evaluation of multi-band systems, where not only the Hall effect³⁰, but also supervening aspects of quantum corrections have to be considered^{39,40}. The logarithmic dependences we find in the progression of the resistance towards lower temperatures are analyzed and quantitatively described by the quantum corrections discussed in Sec. III. In the following, we show data obtained on a $d_{\text{BPO}} = 4.8$ nm thick BaPbO₃ thin film sample acting as a typical representative. In Appendix B, the same data analysis is shown for a thicker sample with $d_{\text{BPO}} = 21.3$ nm, confirming our results.

A. Analysis of Magnetoresistance

The magnetoresistance data are positive for small magnetic fields and display a distinct WAL maximum at $B \sim 0.8$ T, see Fig. 1(a). Fits using Eq. (8) describe the data over the full measured magnetic field range, indicating a triple spin winding. The maximum value of the extracted spin–orbit field is given by $B_{\text{so}} = 0.24$ T.

The second fitting parameter is the inelastic scattering field B_i . At temperatures as high as 70 K, B_i clearly exceeds B_{so} , accessing the WL regime, see Fig. 1(b). Here the magnetoresistance is steadily decreasing for all magnetic fields. Below, the WAL quantum correction can be extracted for temperatures up to 25 K, which we use as a reference temperature T_{ref} in the following analysis. We estimate the temperature dependence of B_i up to T_{ref} to be described by an exponent $\alpha = 1.58$ as well as by a constant contribution for zero temperature, $\gamma = 17$ mT, see Fig. 1(c). The exponent we find is in the typical range for two-dimensional systems, located in the crossover regime between the linear temperature dependence ($\alpha = 1$) due to dephasing by electron–electron scattering at very low temperatures and due to dephasing by electron–phonon scattering ($\alpha \geq 2$) at slightly higher temperatures^{41,42}. Note that the matching of our data with Eq. (8) is a strong indication for single channel transport^{43,44}.

Before proceeding with the analysis of the temperature dependence of the sheet resistance, we like to discuss the unambiguousness of our WAL analysis. Positive magnetoresistance typically results from several origins: (a) multi-carrier Hall effect, (b) magnetism, (c) superconducting fluctuations^{45–47}, (d) EEI^{11,12,38}, or (e) WAL.

A multi-carrier Hall effect (a) does not only affect the sheet resistance, but also most prominently the Hall measurement in form of non-linear contributions. However, as already addressed above, the Hall signal is linear in all of our samples even up to 14 T (see Appendix A) and a multi-carrier effect can be excluded. There is also no obvious signature of magnetism in our samples (b), e.g.,

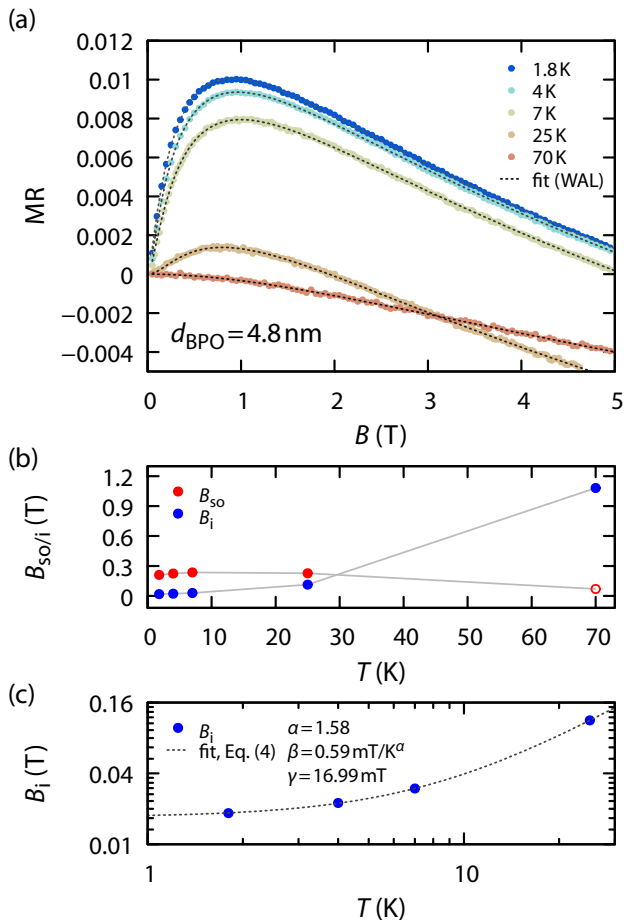


FIG. 1. Exemplary magnetoresistance (MR) data and fit parameters taken and retrieved from a 4.8 nm thick BaPbO₃ thin film grown on a (001) oriented SrTiO₃ substrate. (a) Temperature-dependent magnetoresistance as function of an applied external magnetic field. The dotted lines are fits modeling the quantum corrections following Eq. (8). (b) Extracted spin-orbit fields B_{so} (red) and inelastic fields B_i (blue). At low temperatures B_{so} is clearly larger than B_i with maximum values reaching 0.24 T. At high temperatures $B_i \gg B_{\text{so}}$, therefore the fitted value of B_{so} loses its significance (red circle). Gray lines are guides to the eye. (c) Temperature dependence of the inelastic magnetic field B_i following Eq. (4).

no hysteresis is observed in magnetotransport. In addition, we see no indications for superconductivity even at temperatures as low as 1.8 K, therefore an imprint of superconducting fluctuations (c) is hardly probable. It remains to differentiate the impact of EEI (d) versus WAL (e) on magnetotransport.

The appearance of sizable EEI has been reported in several oxide heterostructures, in particular along with positive magnetoresistance⁴⁸. However, this quantum correction provides a distinct magnetic field behavior in two dimensions: the increase of resistance is quadratic and positive in small magnetic fields and logarithmically

increasing for higher fields, see Eq. (11). The observed distinct maximum with a decreasing or even negative resistance for higher magnetic fields cannot be explained in the scope of EEI.

A combination of WL and EEI quantum corrections has been discussed in two-dimensional semiconductor structures and metallic thin films^{49–53}. Pronounced EEI together with a rather suppressed WL contribution could in principle resemble the observed MR progression. However, our MR data cannot be fitted with physically meaningful parameters by using a combination of WL and EEI quantum corrections.

Any interaction contribution in the magnetotransport data must therefore be much smaller than the quantum interference contribution. Furthermore, the amplitude of the observed magnetoresistance is rather large: the WAL fits provide values of the inelastic scattering field of $B_i \sim 20 \text{ mT}$ for low temperatures (see Fig. 1). Considering Eq. (9), this corresponds to a prefactor that is several orders of magnitudes higher than any realistic prefactor in Eq. (11), where $\bar{B} \sim 1$ for the relevant temperature regime.

Therefore, WAL (e) is the dominant effect that is in agreement with our magnetotransport data, reinforced by the perfect viability of the WAL fits with their realistic fitting parameters.

B. Analysis of Sheet Resistance

Now we turn to the temperature dependence of the resistance. The sheet resistance shows a minimum for an intermediate temperature regime (around 50 K) and increases for decreasing temperature (see Fig. 2). The minimum can be well explained by thermally activated dislocation scattering⁴⁸. An additional sheet resistance increase for lower temperatures, however, is not anticipated from the magnetoresistance analysis. The WAL in the regime $B_{\text{so}} \gg B_i$ for temperatures below $T_{\text{ref}} = 25 \text{ K}$ is associated with a quantum correction that describes a decrease of resistance jointly with temperature, raising the expectation for a metallic ground state. Furthermore, as we observe only one conduction channel (see Appendix A), a simultaneous occurrence of WL accompanied by WAL is hardly probable.

As shown in Sec. III, the magnetoresistance for fixed temperature and the temperature-dependent resistance for fixed field (i. e. zero magnetic field) are described by the same analytical expression. As we have excluded further effects contributing to the magnetoresistance, we extrapolate the quantum correction,

$$\Delta\sigma^{\text{QI}}(B, B_i(T), B_{\text{so}}) = \delta\sigma^{\text{QI}}(B, B_i(T), B_{\text{so}}) - \delta\sigma^{\text{QI}}(0, B_i(T_{\text{ref}}), B_{\text{so}}), \quad (12)$$

to zero magnetic field, see Fig. 3. Here we use the spin-orbit field $B_{\text{so}} = 0.25 \text{ T}$ as extracted from MR data and $T_{\text{ref}} = 25 \text{ K}$ as the reference temperature. This extrap-

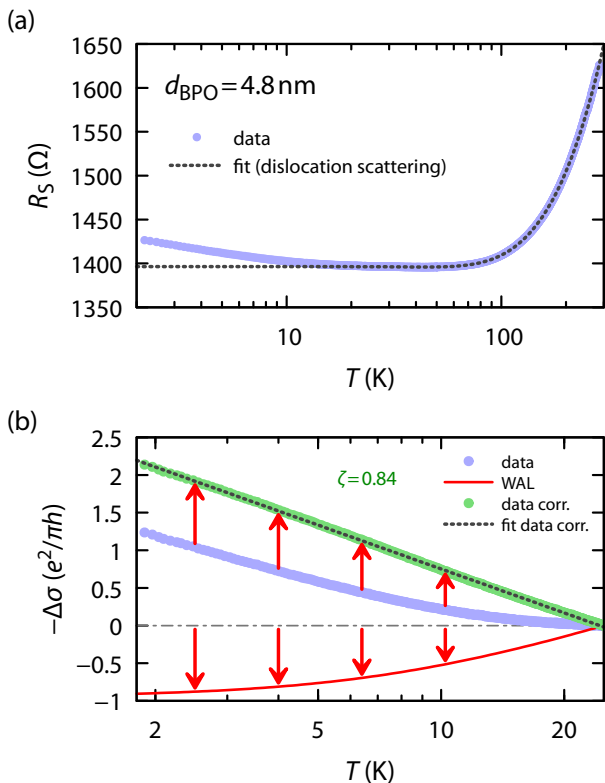


FIG. 2. (a) Observed dependence of the sheet resistance (R_S) on temperature. The progression can be understood in terms of electron–phonon scattering at high temperatures, but is also dominated by dislocation scattering⁴⁸. (b) The progression of the change in conductivity in respect to the reference temperature $T_{\text{ref}} = 25$ K in logarithmic scale (blue data). Following the WAL analysis, a metallic ground state is expected (red line). Reevaluating the data by subtraction of the WAL contribution (red arrows) reveals a logarithmic progression (green data corr.). The fit of this progression is in excellent agreement with weakly screened EEI.

olated WAL contribution is then subtracted from the measured temperature dependent resistances. With this adjustment, a positive logarithmic temperature dependence at low temperatures is uncovered, see Fig. 2 (b). A fit of the resulting progression using the EEI correction, Eq. (10), provides a screening factor of $\zeta = 0.84$, which corresponds to weak screening and is in good agreement with charge carrier densities of 10^{12} cm^{-2} , extracted in Hall measurements (see Appendix A).

Seemingly contradicting logarithmic dependences have also been discussed recently in the literature, e. g., in single crystal thin films of Bi_2Se_3 ^{54,55}. In these topological systems, a combination of two-dimensional quantum corrections of WAL and EEI has been used to describe the measured data. However, we like to emphasize several aspects that are notably different in our data. First, the Bi_2Se_3 samples show a multi-band signature in both the Hall as well the magnetoresistance data, but this signature has not been treated in this framework. In our case

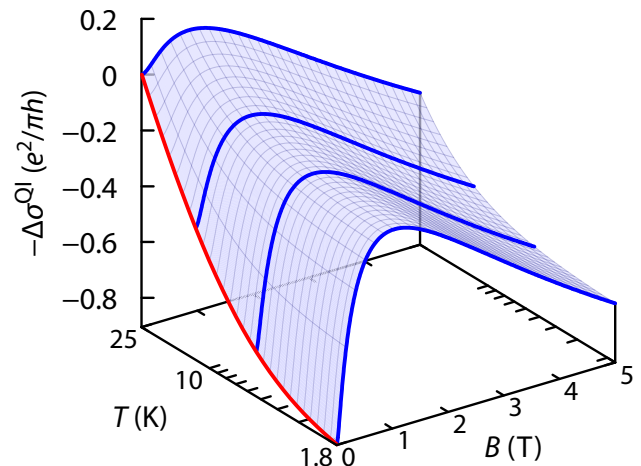


FIG. 3. Progression of the negative conductivity correction over temperature T and magnetic field B following Eq. (12) in respect to the chosen reference temperature $T_{\text{ref}} = 25$ K and setting $B_{\text{so}} = 0.24$ T as extracted from the fits. The blue lines indicate where data are taken in magnetoresistance measurements. We extrapolate the magnetoconductivity to the case $B = 0$ (red line). This is the corresponding WAL quantum correction for zero magnetic field.

we find a clear single-band behavior instead. Secondly, the Bi_2Se_3 magnetotransport data have been discussed for magnetic fields considerably smaller than the field that corresponds to the hypothetical WAL maximum. We stress that our data cannot be explained over the full measured field range with this approach: the negative magnetoresistance for large fields, which is a main feature of quantum interference, is not captured by such an analysis. As far as we know, this issue is still not solved in more recent analyses, where the properties in higher magnetic fields are neglected^{43,56}.

With the data evaluation suggested in this article, we consistently explain the magnetic field and temperature dependence jointly over the full accessible measured ranges: Even when EEI is not pronounced in magnetotransport, it nonetheless plays a dominant role in the temperature dependence of the sheet resistance. Especially in the case of weak screening, i. e., $\zeta \sim 1$, the magnetic field dependence in Eq. (11) vanishes, whereas the logarithmic temperature effect from EEI in Eq. (10) persists. The magnetoresistance even shows an amplitude that exceeds the possible range of the EEI contribution independently of the screening effect by several orders of magnitude. Nevertheless, the screening has a strong impact on the temperature dependence of the sheet resistance.

V. SUMMARY

In conclusion, we investigated electronic transport in thin films of BaPbO_3 down to low temperatures and up to high magnetic fields. The large amplitude observed in the magnetoresistance as well as the distinct maximum cannot be explained within the scope of electron–electron interaction, but are both perfectly described by weak antilocalization with strong spin–orbit coupling as well as weak inelastic scattering.

Our analysis had a clear course of action: first, we analyzed the temperature dependence of the weak antilocalization correction in our magnetoresistance data. From there, we determined the sheet resistance by extrapolation to the respective zero magnetic field contribution of the magnetoresistance. This zero magnetic field behavior, however, does not provide a simple logarithmic temperature dependence due to the finite inelastic field B_i at zero temperature. Only the data that are adjusted by subtraction of the weak antilocalization contribution display a plain logarithmic temperature dependence. This logarithmic dependence can in turn be interpreted with quantum corrections that result from electron–electron interaction for a weakly screened case, despite the negligible influence of interactions in the magnetoresistance. Therefore, quantum corrections due to a mostly unscreened electron–electron interaction together with weak antilocalization provide a full quantitative understanding of our measured transport data.

The lack of screening suppresses the effect of electron–electron interaction even further in the magnetoresistance (Eq. (11)), but its impact on the ground state of the electronic system is rather crucial. In the investigated BaPbO_3 films, the almost unscreened interaction is found to result in a positive contribution to the resistance for low temperatures—preempting a non-metallic state in spite of weak antilocalization.

Further investigations are needed to study the screening in these systems. Control of screening will allow to fine-tune the effect of electron–electron interaction to a scenario where $\zeta \lesssim 1/2$, that is, where weak antilocalization predominates and the ground state is expected to be metallic. Further, we consider it worthwhile to investigate these specific properties of BaPbO_3 also in oxide heterostructures such as $\text{BaPbO}_3\text{--BaBiO}_3$ ¹⁹, where BaPbO_3 is in close vicinity to a charge-ordered insulator, or in interference with helical surface states of topological thin films.

ACKNOWLEDGMENTS

We thank Miriam Stroesser and Marcus Albrecht for helpful discussions and their support in the measurement of the magnetoresistance and Hall data. This work was supported by the Deutsche Forschungsgemeinschaft (DFG, German Research Foundation) – Grant number 107745057 – TRR 80.

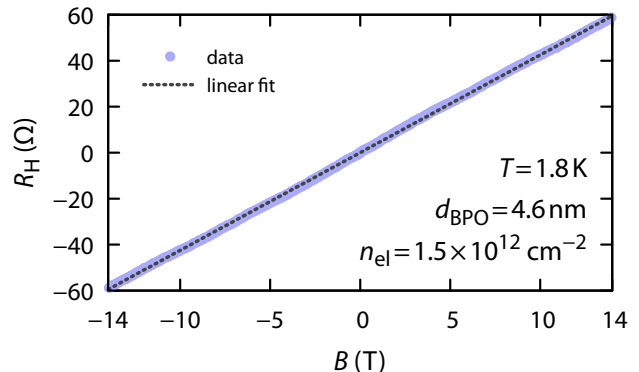


FIG. 4. Exemplary measurement of the Hall resistance (R_H) as function of magnetic field of a $d_{\text{BPO}} = 4.6$ nm thick BaPbO_3 thin film grown by pulsed laser deposition (PLD). The Hall resistance R_H depends linearly on the wide applied magnetic field strongly suggesting single-band behavior. The surface charge carrier density extracted from the linear fit (dashed line) calculates to $n_{\text{el}} = 1.5 \times 10^{12} \text{ cm}^{-2}$ at 1.8 K.

Appendix A: Hall Measurement

Hall measurements in several samples of BaPbO_3 thin films show a linear behavior, suggesting a single type of charge carriers in our systems. An exemplary measurement for a 4.6 nm thick BaPbO_3 thin film up to 14 T is provided in Fig. 4.

Appendix B: Data Analysis of a 21.3 nm BaPbO_3 Thin Film

The same data analysis procedure as shown in the main text also holds for other samples. We show exemplarily the results for a sample of a BaPbO_3 thin film of thickness 21.3 nm. The spin–orbit field is smaller in the thicker sample as it has been in the thinner sample discussed in the main text, see Fig. 5. Again, the extrapolation of the weak antilocalization to zero fields allows to subtract the effect of quantum interference from the temperature dependent measurements, see Fig. 6. The remaining logarithmic increase of the resistance towards lower temperatures can be allocated unambiguously to EEI. In this case, the screening is nearly completely vanishing described by $\zeta = 0.97$.

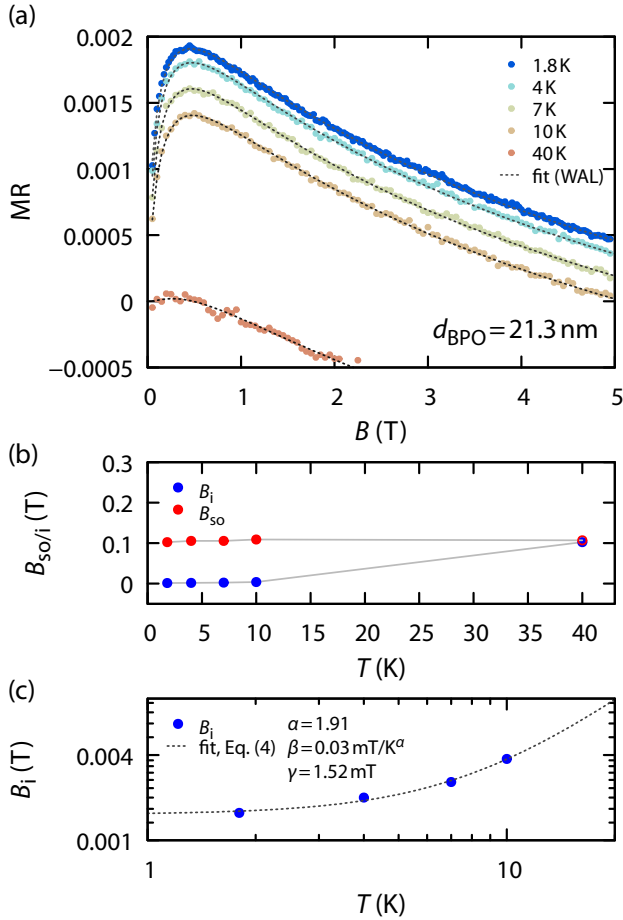


FIG. 5. Exemplary magnetoresistance (MR) data and fit parameter following Fig. 1, taken and retrieved from a 21.3 nm thick BaPbO₃ thin film grown on a (001) oriented SrTiO₃ substrate showing a maximum value of $B_{\text{so}} = 0.11 \text{ T}$.

* german.hammerl@physik.uni-augsburg.de

¹ E. Y. Tsymlal, E. R. A. Dagotto, C.-B. Eom, and R. Ramesh, eds., *Multifunctional Oxide Heterostructures* (Oxford University Press, Oxford, New York, 2012).

² J. K. Freericks, *Transport in multilayered nanostructures*, 2nd ed. (Imperial College Press, 2016).

³ P. Zubko, S. Gariglio, M. Gabay, P. Ghosez, and J.-M. Triscone, Interface physics in complex oxide heterostructures, *Annual Review of Condensed Matter Physics* **2**, 141 (2011).

⁴ R. Hesper, L. H. Tjeng, A. Heeres, and G. A. Sawatzky, Photoemission evidence of electronic stabilization of polar surfaces in K₃C₆₀, *Physical Review B* **62**, 16046 (2000).

⁵ S. Okamoto and A. J. Millis, Electronic reconstruction at an interface between a mott insulator and a band insulator, *Nature* **428**, 630 (2004).

⁶ H. Y. Hwang, Y. Iwasa, M. Kawasaki, B. Keimer, N. Nagaosa, and Y. Tokura, Emergent phenomena at oxide interfaces, *Nature Materials* **11**, 103 (2012).

⁷ E. Rashba, Properties of semiconductors with an extremum loop. 1. cyclotron and combinational resonance in a magnetic field perpendicular to the plane of the loop, *Sov. Phys. Solid St.* **2**, 1109 (1960).

⁸ S. Hikami, A. I. Larkin, and Y. Nagaoka, Spin-orbit interaction and magnetoresistance in the two dimensional random system, *Progress of Theoretical Physics* **63**, 707 (1980).

⁹ J. D. Sau, R. M. Lutchyn, S. Tewari, and S. Das Sarma, Generic new platform for topological quantum computation using semiconductor heterostructures, *Physical Review Letters* **104**, 040502 (2010).

¹⁰ F. Loder, A. P. Kampf, and T. Kopp, Route to topological superconductivity via magnetic field rotation, *Scientific Reports* **5**, 15302 (2015).

¹¹ B. L. Al'tshuler, D. E. Khmel'nitzkii, A. I. Larkin, and P. A. Lee, Magnetoresistance and hall effect in a disordered two-dimensional electron gas, *Phys. Rev. B* **22**, 5142 (1980).

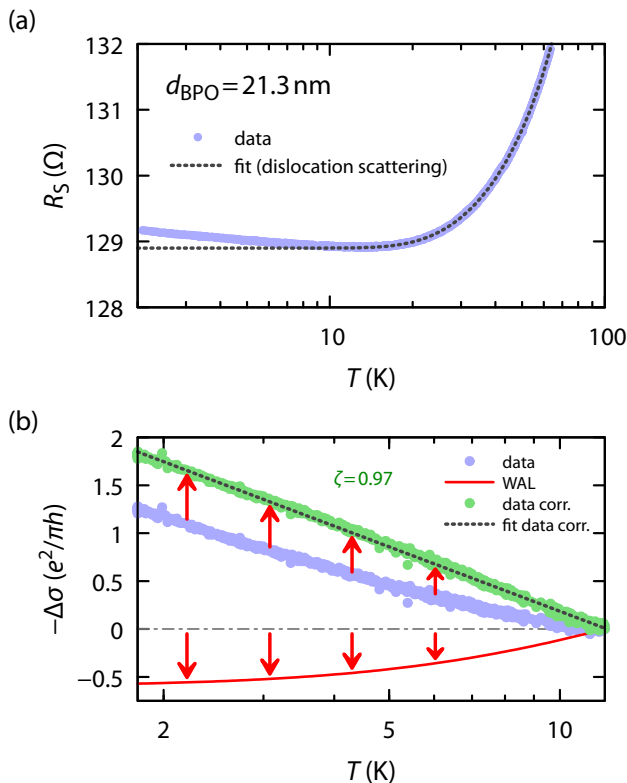


FIG. 6. (a) Exemplary observed dependence of the sheet resistance (R_S) on temperature retrieved for a $d_{\text{BPO}} = 21.3$ nm thick BaPbO_3 sample, following Fig. 2. (b) The analysis follows the procedure described in the main text with chosen reference temperature $T_{\text{ref}} = 12$ K and reveals almost completely unscreened EEI modeled by $\zeta = 0.97$.

¹² P. A. Lee and T. V. Ramakrishnan, Disordered electronic systems, *Rev. Mod. Phys.* **57**, 287 (1985).
¹³ E. Abrahams, P. W. Anderson, D. C. Licciardello, and T. V. Ramakrishnan, Scaling theory of localization: Absence of quantum diffusion in two dimensions, *Phys. Rev. Lett.* **42**, 673 (1979).
¹⁴ F. Wegner, The mobility edge problem: Continuous symmetry and a conjecture, *Zeitschrift für Physik B Condensed Matter* **35**, 207 (1979).
¹⁵ F. Wegner, Four-loop-order β -function of nonlinear σ -models in symmetric spaces, *Nuclear Physics B* **316**, 663 (1989).
¹⁶ S. V. Iordanskii, Y. B. Lyanda-Geller, and G. E. Pikus, Weak localization in quantum wells with spin-orbit interaction, *Pis'ma Zh. Eksp. Teor. Fiz.* **60**, 199 (1994), [*JETP Lett.* **60**, 206 (1994)].
¹⁷ B. Yan, M. Jansen, and C. Felser, A large-energy-gap oxide topological insulator based on the superconductor BaBiO_3 , *Nature Physics* **9**, 709 (2013).
¹⁸ G. Li, B. Yan, R. Thomale, and W. Hanke, Topological nature and the multiple dirac cones hidden in bismuth high- T_c superconductors, *Scientific Reports* **5**, 10435 (2015).
¹⁹ B. Meir, S. Gorol, T. Kopp, and G. Hammerl, Observation of two-dimensional superconductivity in bilayers of BaBiO_3 and BaPbO_3 , *Physical Review B* **96**, 100507(R) (2017).

²⁰ D. E. Cox and A. W. Sleight, Crystal structure of $\text{Ba}_2\text{Bi}^{3+}\text{Bi}^{5+}\text{O}_6$, *Solid State Communications* **19**, 969 (1976).
²¹ D. E. Cox and A. W. Sleight, Mixed-valent $\text{Ba}_2\text{Bi}^{3+}\text{Bi}^{5+}\text{O}_6$: Structure and properties vs temperature, *Acta Crystallographica Section B: Structural Crystallography and Crystal Chemistry* **35**, 1 (1979).
²² C. M. Varma, Missing valence states, diamagnetic insulators, and superconductors, *Physical Review Letters* **61**, 2713 (1988).
²³ V. V. Bogato and Y. N. Venvtsev, Superconductivity of BaPbO_3 , *Sov. Phys. Solid St.* **22**, 705 (1980).
²⁴ M. Kawasaki, K. Takahashi, T. Maeda, R. Tsuchiya, M. Shinohara, O. Ishiyama, T. Yonezawa, M. Yoshimoto, and H. Koinuma, Atomic control of the SrTiO_3 crystal surface, *Science* **266**, 1540 (1994).
²⁵ G. Koster, B. L. Kropman, G. J. H. M. Rijnders, D. H. A. Blank, and H. Rogalla, Quasi-ideal strontium titanate crystal surfaces through formation of strontium hydroxide, *Applied Physics Letters* **73**, 2920 (1998).
²⁶ M. D'yakonov and V. Perel, Spin orientation of electrons associated with the interband absorption of light in semiconductors, *Zh. Eksp. Teor. Fiz.* **60**, 1954 (1971), [*JETP* **33**, 1053 (1971)].
²⁷ G. Bergmann, Weak localization in thin films: A time-of-flight experiment with conduction electrons, *Physics Reports* **107**, 1 (1984).
²⁸ H. Nakamura, T. Koga, and T. Kimura, Experimental evidence of cubic Rashba effect in an inversion-symmetric oxide, *Phys. Rev. Lett.* **108**, 206601 (2012).
²⁹ Y. Kim, R. M. Lutchyn, and C. Nayak, Origin and transport signatures of spin-orbit interactions in one- and two-dimensional SrTiO_3 -based heterostructures, *Phys. Rev. B* **87**, 245121 (2013).
³⁰ P. Seiler, J. Zabaleta, R. Wanke, J. Mannhart, T. Kopp, and D. Braak, Antilocalization at an oxide interface, *Phys. Rev. B* **97**, 075136 (2018).
³¹ Y.-Y. Pai, A. Tylan-Tyler, P. Irvin, and J. Levy, Physics of SrTiO_3 -based heterostructures and nanostructures: a review, *Reports on Progress in Physics* **81**, 036503 (2018).
³² F. G. Pikus and G. E. Pikus, Conduction-band spin splitting and negative magnetoresistance in A_3B_5 heterostructures, *Phys. Rev. B* **51**, 16928 (1995).
³³ W. Knap, C. Skierbiszewski, A. Zduniak, E. Litwin-Staszewska, D. Bertho, F. Kobbi, J. L. Robert, G. E. Pikus, F. G. Pikus, S. V. Iordanskii, V. Mosser, K. Zekentes, and Y. B. Lyanda-Geller, Weak antilocalization and spin precession in quantum wells, *Phys. Rev. B* **53**, 3912 (1996).
³⁴ M. D'yakonov and V. Perel, Spin relaxation of conduction electrons in noncentrosymmetric semiconductors, *Soviet Physics Solid State, USSR* **13**, 3023 (1972).
³⁵ P. Mohanty, E. M. Q. Jariwala, and R. A. Webb, Intrinsic decoherence in mesoscopic systems, *Phys. Rev. Lett.* **78**, 3366 (1997).
³⁶ P. Mohanty and R. A. Webb, Decoherence and quantum fluctuations, *Phys. Rev. B* **55**, R13452 (1997).
³⁷ Y. Imry, Dephasing by coupling with the environment, application to coulomb electron-electron interaction in metals, in *Introduction to mesoscopic physics* (Oxford University Press, 2008) 2nd ed., pp. 32–57.
³⁸ B. L. Altshuler, A. G. Aronov, and P. A. Lee, Interaction effects in disordered Fermi systems in two dimensions, *Phys. Rev. Lett.* **44**, 1288 (1980).

- ³⁹ P. Seiler, E. Lettl, D. Braak, and T. Kopp, Antilocalization in oxides: Effective spin-3/2 model, *Phys. Rev. B* **100**, 121404(R) (2019).
- ⁴⁰ P. Seiler, E. Lettl, D. Braak, and T. Kopp, Weak antilocalization within a genuine multiband model, *Physical Review B* **100**, 115415 (2019).
- ⁴¹ E. Abrahams, P. W. Anderson, P. A. Lee, and T. V. Ramakrishnan, Quasiparticle lifetime in disordered two-dimensional metals, *Physical Review B* **24**, 6783 (1981).
- ⁴² J. J. Lin and J. P. Bird, Recent experimental studies of electron dephasing in metal and semiconductor mesoscopic structures, *Journal of Physics: Condensed Matter* **14**, R501 (2002).
- ⁴³ H.-Z. Lu and S.-Q. Shen, Finite-temperature conductivity and magnetoconductivity of topological insulators, *Phys. Rev. Lett.* **112**, 146601 (2014).
- ⁴⁴ J. Liao, Y. Ou, H. Liu, K. He, X. Ma, Q.-K. Xue, and Y. Li, Enhanced electron dephasing in three-dimensional topological insulators, *Nature Communications* **8**, 16071 (2017).
- ⁴⁵ L. G. Aslamasov and A. I. Larkin, The influence of fluctuation pairing of electrons on the conductivity of normal metal, *Physics Letters A* **26**, 238 (1968).
- ⁴⁶ K. Maki, Critical fluctuation of the order parameter in a superconductor. I, *Progress of Theoretical Physics* **40**, 193 (1968).
- ⁴⁷ R. S. Thompson, Microwave, flux flow, and fluctuation resistance of dirty type-II superconductors, *Phys. Rev. B* **1**, 327 (1970).
- ⁴⁸ D. Fuchs, A. Sleem, R. Schäfer, A. G. Zaitsev, M. Meffert, D. Gerthsen, R. Schneider, and H. v. Löhneysen, Incipient localization of charge carriers in the two-dimensional electron system in $\text{LaAlO}_3/\text{SrTiO}_3$ under hydrostatic pressure, *Phys. Rev. B* **92**, 155313 (2015).
- ⁴⁹ D. A. Poole, M. Pepper, and R. W. Glew, The observation of localisation and interaction effects in the two-dimensional electron gas of a GaAs-GaAlAs heterojunction at low temperatures, *J. Phys. C: Solid State Phys.* **14**, L995 (1981).
- ⁵⁰ D. J. Bishop, R. C. Dynes, and D. C. Tsui, Magnetoresistance in Si metal-oxide-semiconductor field-effect transistors: Evidence of weak localization and correlation, *Phys. Rev. B* **26**, 773 (1982).
- ⁵¹ B. J. F. Lin, M. A. Paalanen, A. C. Gossard, and D. C. Tsui, Weak localization of two-dimensional electrons in GaAs - $\text{Al}_x\text{Ga}_{1-x}\text{As}$ heterostructures, *Phys. Rev. B* **29**, 927 (1984).
- ⁵² G. Bergmann, Quantum corrections to the resistance in two-dimensional disordered superconductors above T_c : Al, Sn, and amorphous $\text{Bi}_{0.9}\text{Tl}_{0.1}$ films, *Phys. Rev. B* **29**, 6114 (1984).
- ⁵³ R. Taboryski and P. E. Lindelof, Weak localisation and electron-electron interactions in modulation-doped GaAs/AlGaAs heterostructures, *Semicond. Sci. Technol.* **5**, 933 (1990).
- ⁵⁴ J. Wang, A. M. DaSilva, C.-Z. Chang, K. He, J. K. Jain, N. Samarth, X.-C. Ma, Q.-K. Xue, and M. H. W. Chan, Evidence for electron-electron interaction in topological insulator thin films, *Phys. Rev. B* **83**, 245438 (2011).
- ⁵⁵ M. Liu, C.-Z. Chang, Z. Zhang, Y. Zhang, W. Ruan, K. He, L.-l. Wang, X. Chen, J.-F. Jia, S.-C. Zhang, Q.-K. Xue, X. Ma, and Y. Wang, Electron interaction-driven insulating ground state in Bi_2Se_3 topological insulators in the two-dimensional limit, *Phys. Rev. B* **83**, 165440 (2011).
- ⁵⁶ R. Sultana, G. Gurjar, P. Neha, S. Patnaik, and V. P. S. Awana, Hikami-Larkin-Nagaoka (HLN) treatment of the magneto-conductivity of Bi_2Te_3 topological insulator, *Journal of Superconductivity and Novel Magnetism* **31**, 2287 (2018).